

Cathode Atomic Structures and Their Electrolyte Interfaces in Lithium-sulfur Batteries

Tanika Duivenvoorden,^[a, b] Stephen Sanderson,^[a] and Debra J. Searles^{*[a, b]}

Lithium-sulfur batteries (LSBs) are a promising alternative to conventional battery technologies due to their high theoretical energy density. However, the insulating nature of sulfur and the polysulfide shuttle effect present practical challenges to achieving this. This study employs molecular dynamics simulations with a ReaxFF reactive force field to investigate the structure of LSB cathode-electrolyte interfaces, with cathode materials made from different sized graphene flakes and elemental sulfur (S_8). Smaller graphene flakes were seen to bond more with the sulfur, while structures with larger graphene flakes featured fewer C–S bonds and more long-chain sulfur species. Observing the interface between the cathode and an organic electrolyte

revealed that cathode structures with larger graphene flakes could orientate to shield the long-chain sulfur and lithium polysulfide species from interacting with and dissolving into the electrolyte. Additional simulations were performed to investigate cathode materials with regions of crystalline α - S_8 . However, it was found that the ReaxFF force field used for LSB systems cannot effectively model crystalline sulfur under constant pressure conditions. Further development of reactive force fields for simulation of graphene flake and sulfur electrodes in the presence of electrolyte are therefore required to explore the full range of likely structures using these methods.

Introduction

Designing and investigating new materials for energy storage devices is important to develop sustainable energy for a range of industrial applications. Finding alternatives to the conventional lithium-ion battery (LIB) is a particularly prevalent area of research aiming to reduce costs and improve battery performance.^[1] Commercially available LIBs with lithium metal oxide cathodes and graphite anodes achieve energy densities of between 150 and 200 Wh kg⁻¹,^[1a,2] with potential improvements providing theoretical energy densities of up to approximately 390 Wh kg⁻¹.^[3] However, even these values are insufficient to support the growing industrial demand of applications such as electric vehicles and electronic grid storage.^[2a] Lithium-sulfur batteries (LSBs) are promising candidates to overtake conventional LIB performance, as their theoretical energy density of 2500–2600 Wh kg⁻¹,^[4,5] is approximately six times higher than the maximum energy density of LIBs. Additionally,

sulfur is naturally abundant, non-toxic, and low cost, making it an ideal cathode material for commercialization.^[3,4]

LSBs are typically made up of a lithium metal anode, an organic electrolyte, a separator, and a cathode material of elemental sulfur (e.g., in the crystalline form of orthorhombic cyclic octasulfur: α - S_8) incorporated into a conductive carbon framework.^[3] The usual electrochemical discharge process involves the Li metal of the anode being oxidized to Li⁺, which then migrates through the electrolyte to react with reduced S_8 at the cathode. This migration creates an ionic and electrical current across the cell. Li⁺ typically reacts at the cathode alongside a series of sulfur reductions which produce polysulfides with progressively shorter chains ($Li_2S_8 \rightarrow Li_2S_6 \rightarrow Li_2S_4 \rightarrow Li_2S_2 \rightarrow Li_2S$).^[1] The overall discharge reaction which provides energy in a LSB cell is:



Although many refer to this in the literature,^[1] the reduction pathway in a carbon framework is less clear and depends on the structure of the sulfur carbon composite. In some studies, authors have reported alternative pathways involving the formation of Li_2S_3 and Li_2S_5 or even the immediate formation of the reduced S²⁻ species.^[6]

Despite their potential advantages, LSBs face several challenges in practice that impact their performance, including cathode expansion,^[7] dendrite formation at the anode,^[8] the insulating nature of sulfur,^[1a] and the polysulfide shuttle effect.^[1b] The polysulfide shuttle effect is caused by the high solubility of long chain polysulfides (Li₂S_n where $n \geq 4$) in commonly used ether-based electrolytes.^[1b] As long chain polysulfides form during discharge, they can dissolve in the electrolyte and “shuttle” across the cell to react at the anode

[a] T. Duivenvoorden, Dr. S. Sanderson, Prof. D. J. Searles
Centre for Theoretical and Computational Molecular Science
Australian Institute for Bioengineering and Nanotechnology
The University of Queensland
Queensland 4072 (Australia)
E-mail: d.bernhardt@uq.edu.au

[b] T. Duivenvoorden, Prof. D. J. Searles
School of Chemistry and Molecular Biosciences
The University of Queensland
Queensland 4072 (Australia)

 Supporting information for this article is available on the WWW under <https://doi.org/10.1002/batt.202300324>

 © 2023 The Authors. *Batteries & Supercaps* published by Wiley-VCH GmbH. This is an open access article under the terms of the Creative Commons Attribution Non-Commercial NoDerivs License, which permits use and distribution in any medium, provided the original work is properly cited, the use is non-commercial and no modifications or adaptations are made.

without providing electrical current, decreasing battery performance (Figure 1).

These drawbacks cause issues with LSB cycle life, stability, and electrochemical activity of the cathode, meaning experimental energy densities (up to 400 Wh kg⁻¹)^[1a] are much lower than theoretical values. A considerable amount of research has aimed to address these problems by optimizing LSB material design.^[1a,5b] This work will focus on the challenges in cathode design associated with elemental sulfur conductivity and the polysulfide shuttle effect.

Sulfur is an insulator (5×10^{-30} S cm⁻¹ at 25 °C),^[4] so to produce an efficient LSB, elemental sulfur must be incorporated into a conductive but electrochemically inert framework to allow for the movement of charge through the electrode.^[4,9] Unfortunately, this decreases the energy density of the cell, but it is essential for improving conductivity and battery performance. Carbon is an ideal element to use as a framework in a range of forms, including microporous carbon, nanoparticles, nanotubes, graphene sheets and graphene flakes, which can all exhibit high conductivity and structural integrity.^[3] Maximizing the surface area and contact between the carbon framework and sulfur while also maximizing the sulfur loading in the cathode has been suggested to improve LSB performance.^[5,10]

Significant experimental and theoretical research has been dedicated to mitigating or preventing the polysulfide shuttle effect to improve LSB performance, by designing new separators or modifying electrolyte compositions.^[11] This has also been integrated with research into cathode material design, with the aim of capturing polysulfides at the cathode as well as maximizing conductivity.^[9,10,11c,12] Combining graphene flakes and elemental sulfur (α -S₈) produces some promising cathode

materials which are kinetically stable, but not thermodynamically stable. This allows for the formation of a broad range of different structures, especially under the varying conditions of temperature and pressure used in different methods of preparation.

As an example of the different structures that can form, some LSB cathode materials have been reported in the literature as an amorphous mixture of sulfur and carbon, featuring sulfur-coated agglomerations of graphene flakes with no significant pores.^[13] These were typically synthesized using melt or vapor infiltration methods. Conversely, other LSB cathode materials have been characterized as having porous interconnected graphene flakes which host roughly spherical sulfur clusters, typically synthesized using ball milling or solution infiltration methods.^[14] X-ray diffraction (XRD) data collected for some of these cathodes suggested crystalline sulfur was still present in the material after formation of the sulfur-carbon composite.^[14a,b]

Structural features of these cathode materials also appear to be highly dependent on the weight percentage (wt%) of sulfur (and thus the ratio of sulfur to carbon). When higher sulfur loadings of 60–80 wt% were used with the melt infiltration method, crystalline regions of α -S₈ were observed in the XRD data even after the melting process.^[13a,b] This could be due to the increased proportion of sulfur compared to the number of binding sites on the edges of the graphene flakes, as at low sulfur loadings (20–40 wt%), structures were highly amorphous with no observable crystalline sulfur.^[13b] Electrochemical testing of a range of cathodes with different sulfur loadings found a sulfur content of 60 wt% had the highest performance in capacity and cycling stability, attributed to the cathode's microstructure and composition.^[13b]

Studying these materials is of interest from both an experimental synthesis and computational simulation perspective. Computational simulations can provide more detail than can be observed experimentally on the precise structure of the system and how it influences properties and reaction mechanisms. Previous literature has reported the simulation and characterization of sulfur and graphene flake cathodes using techniques such as *ab initio* molecular dynamics (AIMD) simulation,^[6b,15] and molecular dynamics (MD) simulation with the reactive force field ReaxFF.^[3,16] Both methods can be used to model the dynamic evolution and reactive events of a system.

Computational literature has revealed information on the sulfur reduction mechanism in both crystalline sulfur systems and composite carbon-sulfur cathode materials. Arneson et al.^[17] used AIMD simulations to model a pure crystalline α -S₈ cathode surface against dimethoxyethane (DME) electrolyte, and then randomly added lithium cations to the interface to simulate the lithiation process. Although this system is useful for pure α -S₈ cathodes, the assumptions are not valid for all systems, as other experimental and computational studies have shown evidence of amorphous carbon-sulfur composites featuring different sulfur species and reduction pathways.^[6a] One such study used MD simulations with ReaxFF to compare a pure α -S₈ cathode to a graphene flake and sulfur composite cathode.^[3] Lithium ions were randomly added to the cathode structures

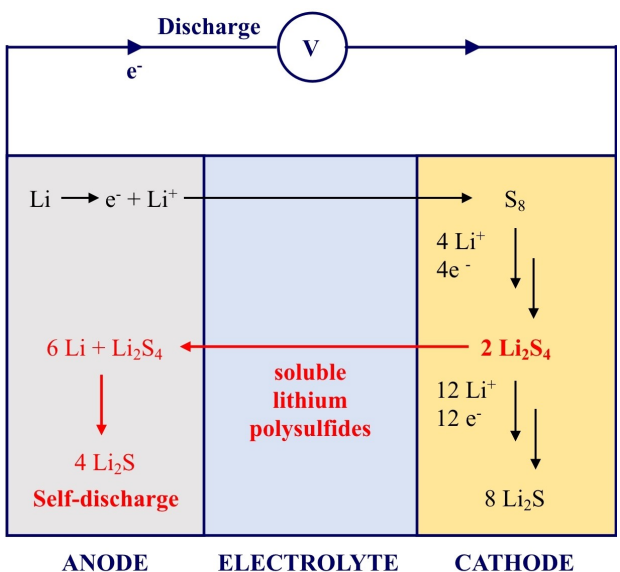


Figure 1. A LSB during discharge. The process in black represents the discharge reduction reaction of elemental sulfur (S₈) forming lithium polysulfides, while the process in red represents the polysulfide shuttle effect leading to self-discharge.

over time to observe the sulfur reduction and lithiation mechanism. The calculated voltage discharge curve of the pure $\alpha\text{-S}_8$ and sulfur-carbon composite materials were different across the lithiation process. Based on these results, the carbon flake material would likely be required to effectively model the sulfur species present, and thus the mechanism of sulfur reduction.

AIMD simulations have also been used in the literature to observe the sulfur reduction mechanism within a 1–2 nm pore between two graphene sheets.^[16b,14b] In these studies, two S_8 molecules were placed at the edge of a pore between two graphene walls, with the surrounding space inside the pore filled with 1,3-dioxolane (DOL) solvent molecules. Li atoms were added randomly within the system's pore to study the sulfur reduction mechanism and formation of polysulfide products. The results indicated alternative pathways were present that contradicted the series of polysulfide reductions which had been previously proposed. Burgos et al.^[16b] further suggested that the pore structure of the system may determine the reaction mechanism and products formed in the sulfur reduction. A similar difference in reactivity has also been observed by Fu et al.^[11c] when polysulfides were confined in different sized carbon nanotubes.

Other computational studies have focused on investigating the structure of lithiated and delithiated cathodes by initially generating a mixture of S_8 rings and graphene flakes and then equilibrating these structures (at room temperature) using MD simulations with ReaxFF.^[3,16] Ponce and Seminario^[16] simulated several systems with C_{42} graphene flakes and various sulfur loadings. In both the lithiated and delithiated structures, S_8 rings opened to form long chain lithium polysulfides, or reacted with the peripheral carbon atoms of the graphene flakes. Perez Beltran and Balbuena^[3] performed a similar structural study, equilibrating a 64 wt% sulfur cathode containing a mixture of C_{16} and C_{22} graphene flakes. After thermal stabilization it was found that S_8 rings broke apart into linear sulfur chains, and randomly placed graphene flakes preferred to stack together to form small graphite-like structures.

Both structures generated using MD simulations with ReaxFF were consistent with experimental cathodes synthesized using the melt diffusion and vapor infiltration methods, where the sulfur coated the edges of the graphene flakes and formed an amorphous material.^[13b,c] However, these simulations have not shown any $\alpha\text{-S}_8$ crystalline regions within a carbon-sulfur composite, despite this structural feature being recorded in several experimental papers.^[13a,b,14a,b] The lack of crystalline sulfur could be an artefact of the computational method used when simulating a randomly distributed mix of graphene flakes and S_8 molecules. If small units of crystalline $\alpha\text{-S}_8$ were randomly distributed instead of individual S_8 molecules, these crystalline regions might remain after thermal stabilization. A structure like this may behave differently to amorphous carbon-sulfur composites and elemental sulfur cathodes regarding the mechanism and products of the sulfur reduction.

This highlights the need for further investigation into which structural features (i.e., of the carbon framework, the different sulfur species present, and the cathode-electrolyte interface)

can be observed in these carbon-sulfur composite systems. Research into how to model different graphene flake and sulfur materials would be beneficial to exploring the possible reaction mechanisms which may occur across a variety of cathode structures. Knowledge of the effect of cathode structure on sulfur reduction and polysulfide behavior can then inform improved cathode design for LSBs.

This work simulated a range of cathode structures formed from graphene flakes and S_8 rings using MD simulation with ReaxFF. The simulated cathodes were prepared with different sized graphene flakes, and with both random dispersion of S_8 molecules and random dispersion of $\alpha\text{-S}_8$ crystal blocks. Additionally, two of the simulated cathode structures were equilibrated alongside a common organic electrolyte of DOL molecules containing randomly distributed Li atoms. The various cathode structures and cathode-electrolyte interfaces were then analyzed to gain insight into the effect of the material structure on sulfur reduction and the polysulfide shuttle effect.

System details

Individual molecules of S_8 , C_{16} , C_{22} and C_{42} were minimized in Avogadro (version 1.2)^[18] using the Merck Molecular Force Field 94 (for octasulfur S_8)^[19] and the Universal Force Field (for graphene flakes C_{16} , C_{22} , and C_{42}).^[20] These are shown in Figure 2. To produce the initial configurations of the cathode systems, these molecules were randomly placed in a simulation box using the Packing Optimization for Molecular Dynamics Simulations (PACKMOL) software.^[21] The cells were packed to an initial density of 1.25 g cm^{-3} with an atom tolerance of 3 \AA to

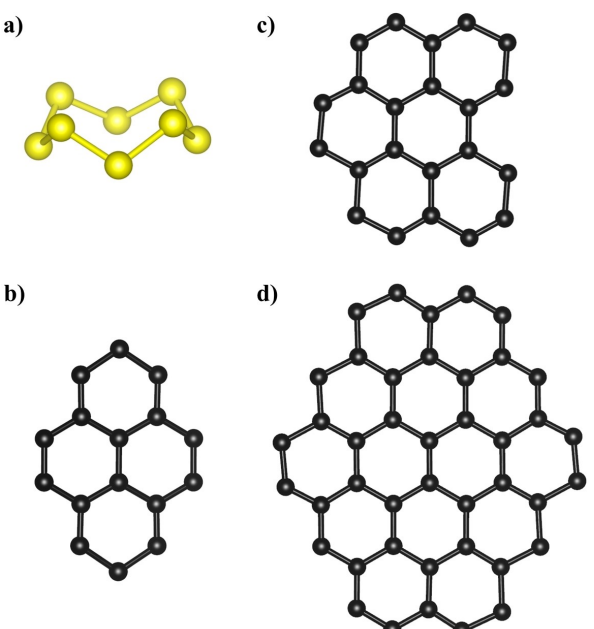


Figure 2. Molecules used to generate initial configurations of cathode materials: a) S_8 , b) C_{16} graphene flake, c) C_{22} graphene flake, d) C_{42} graphene flake.

balance the attractive and repulsive forces before structural relaxation.^[16] Two different cathode structures were studied, with one containing small graphene flakes (C_{16} and C_{22}) and the other containing large graphene flakes (C_{22} and C_{42}). These will be referred to as CAT01 and CAT02, respectively. The components of the two cathodes are presented in Table 1. Both systems contained 64 wt % sulfur as S_8 rings randomly dispersed among the graphene flakes.

MD simulations of the cathode and cathode-electrolyte interfaces with DOL solvent and Li atoms were performed using the ReaxFF force field parameterized by Islam et al.^[22] in the Large-scale Atomic/Molecular Massively Parallel Simulator (LAMMPS, 17 Jan 2018) software.^[23] Additional MD simulations of the cathode systems were also performed using the ReaxFF force field parameterized by Järvi et al.^[24]

Results and Discussion

Modelling cathode-electrolyte interface

The final equilibrated structures of the CAT01 and CAT02 systems and their interfaces with electrolyte are shown in Figure 3. During thermal equilibration, the S_8 rings in the cathode structures (Figure 3a and b) reacted to form either linear sulfur chains of varying lengths, or sulfur-carbon composite molecules where sulfur atoms bonded to the graphene flake edges. Additionally, graphene flakes were observed to form π - π stacking arrangements that resemble small graphite-like structures. The smaller graphene flakes in CAT01 had a higher number of reactive edge sites compared to the larger flakes in CAT02, which allowed for more C–S bonds to form in the equilibrated CAT01 structure. The S_8 molecules in the equilibrated CAT02 structure preferred to bond to each other, producing long chain sulfur species, and forming fewer bonds to the graphene flakes.

The CAT01 and CAT02 cathode-electrolyte surfaces were formed via equilibration with the ReaxFF force field parameterized by Islam et al.^[22] (Figure 3c and d). During the CAT01 interfacial relaxation, the cathode and electrolyte regions came together rapidly to interact and form an interface. As this interface continued to equilibrate, some electrolyte molecules and Li atoms were observed to penetrate the cathode structure (Figure 3c). Likewise, some sulfur-coated fragments of graphene flakes were seen to migrate into the electrolyte more than

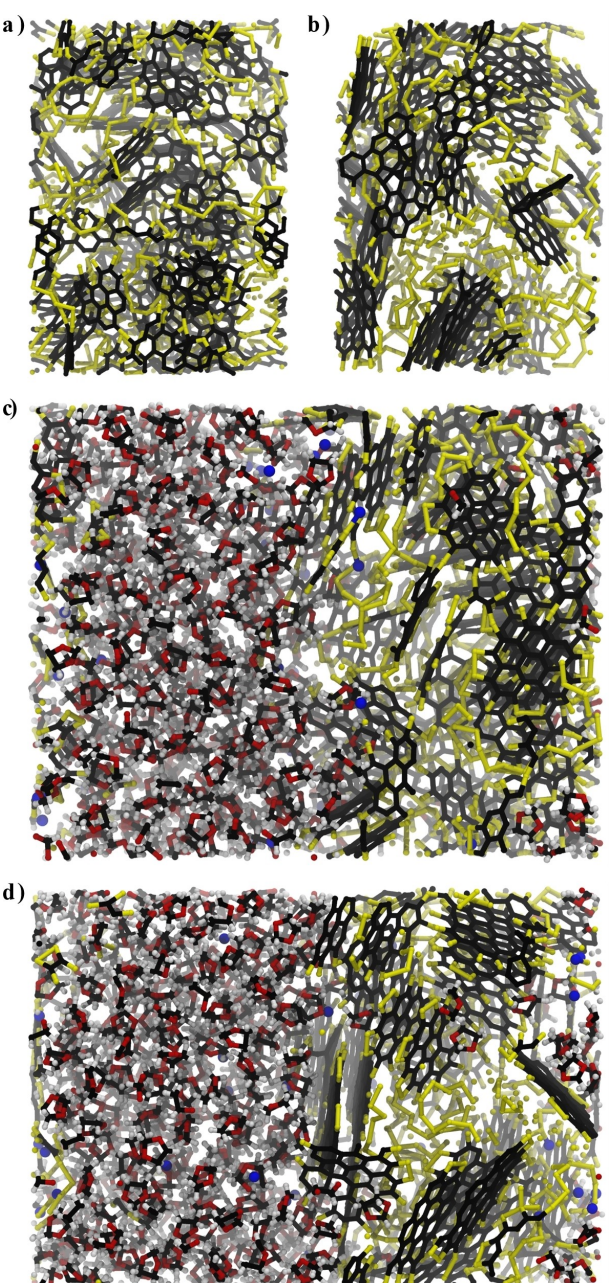


Figure 3. The equilibrated structures of a) CAT01, b) CAT02, c) CAT01 interface with DOL electrolyte, d) CAT02 interface with DOL electrolyte. All structures were equilibrated using the ReaxFF force field parameterized by Islam et al.^[22] Atoms represented by different colors, C: black, S: yellow, H: white, O: red, and Li: blue.

Table 1. Composition of systems used in molecular dynamics simulations.

System name*	Initial box dimensions [Å]	System composition	
CAT01	49×42×30	37	C_{16}
		37	C_{22}
		116	S_8
CAT02	49×42×30	22	C_{22}
		22	C_{42}
		116	S_8

*CAT refers to cathode (sulfur plus graphene) systems.

others, creating a slightly rough surface. For the CAT02 surface, similar interfacial interactions were observed. However, some of the larger graphene flakes at the interface adopted orientations which blocked the migration of electrolyte molecules into the cathode and appeared to prevent the sulfur chains in the cathode from interacting with the electrolyte (Figure 3d). While some flakes in the CAT01 system also adopted face-on orientations with the electrolyte, these flakes were too small to effectively block sulfur chains from interacting with the electrolyte.

The radial distribution functions (RDFs) of lithium with the carbon of the cathode structures ($\text{Li}-\text{C}_{\text{CAT}}$) for CAT01 and CAT02 are presented in Figure 4(a). These results show that more lithium atoms were interacting with the carbon atoms of CAT01 than CAT02, suggesting that the lithium penetration into the cathode was higher for the structure with smaller graphene flakes. The RDFs of the lithium and sulfur interactions are presented in Figure 4(b). The CAT01 RDF exhibits a slightly higher first shell interaction between lithium and sulfur at 2.4 Å, while the CAT02 RDF shows a much higher second shell interaction between lithium and sulfur at 3.7 Å. It is likely that the lithium bonded to sulfur in the CAT01 structure is mostly anchored directly to the graphene flakes ($\text{C}-\text{S}-\text{Li}$) due to the increased number of graphene flake edge sites and sulfur carbon bonds in this structure. This would explain the lack of a high second-shell $\text{Li}-\text{S}$ interaction in Figure 4(b). The CAT02 structure with larger graphene flakes had fewer reactive edge sites and more long-chain sulfur, and so had a higher number of lithium bonding with sulfur chains, producing the larger second shell peak in Figure 4(b).

Molecule population analysis of the surface structures present at the end of the thermal equilibration was performed using TRAVIS – Trajectory Analyser and Visualiser.^[34] These results also identified that the number of $\text{Li}-\text{S}$ bonds was slightly higher in the CAT01 system than the CAT02 system.

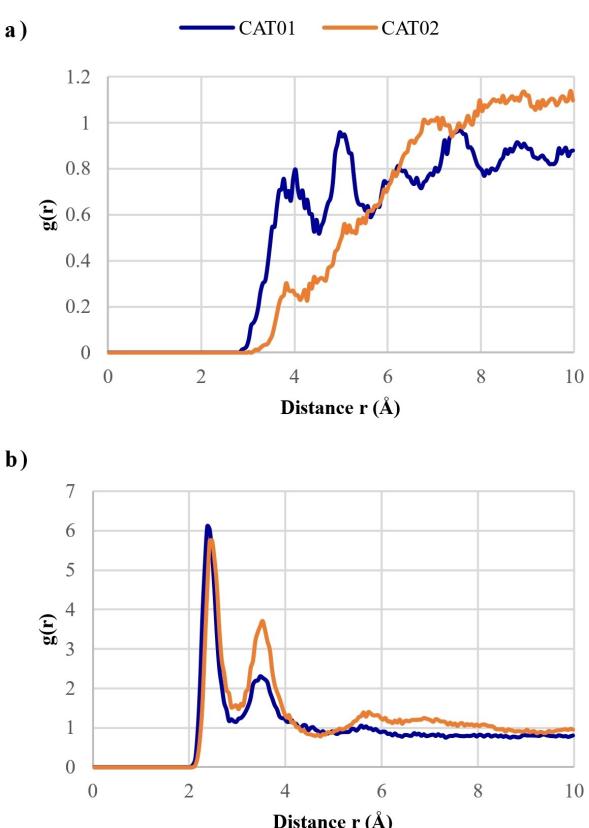


Figure 4. RDFs of the a) $\text{Li}-\text{C}_{\text{CAT}}$ and b) $\text{Li}-\text{S}$ interactions for the CAT01 and CAT02 cathode-electrolyte interfaces. C_{CAT} refers to carbon atoms in the cathode structure (does not include carbons in the electrolyte DOL molecules).

Additionally, the CAT02 system had a larger number of long chain Li polysulfides which were not anchored to the graphene flakes compared to the CAT01 structure. These results suggest the CAT01 structure with smaller graphene flakes would be more conductive, as the sulfur was more bonded and dispersed within the graphene flake framework. The increased number of $\text{C}-\text{S}$ bonds at the graphene flake edges of CAT01 could also potentially decrease the polysulfide shuttle effect, as the polysulfide species which form would be anchored to the carbon framework.^[9] Conversely, the larger graphene flakes of CAT02 provided a physical barrier at the interface to prevent sulfur chains from migrating into the electrolyte. This resembles a more porous carbon framework which could also potentially help prevent the polysulfide shuttle effect.^[1b,9] During these simulations, no polysulfide shuttle was observed through the electrolyte. As such, additional simulations with longer time-scales or with an electric field applied would be required to determine which structure of CAT01 or CAT02 would be more effective in preventing the polysulfide shuttle effect.

ReaxFF force field comparison

The cathode structures presented above exhibited similar characteristics to experimental Li–S battery cathodes that were synthesized using melt infiltration methods, where the sulfur coated onto the graphene flake and graphite structure edges.^[13b,c] However, no structures were observed to have any crystalline sulfur, despite this often being observed in experimental cathodes made using a high sulfur content or mechanical intrusion methods.^[13a,b,14a,b] Indeed, not only was there no crystalline sulfur, but all the elemental S_8 ring structures reacted to form an amorphous mixture of graphene flakes and sulfur chains.

To produce a computational model of a cathode structure more applicable to experimental systems with crystalline sulfur, a crystalline α -sulfur ($\alpha\text{-S}_8$) supercell was equilibrated with the same force field. During this equilibration, it was found that the systems simulated using the Islam et al.^[22] force field would maintain crystallinity during the NVT stage, but the crystalline structure then collapsed upon applying NPT conditions (Figure 5a). It appeared that the force field was calculating a very high average pressure for the initial crystal structure coordinates. Several variations to the method were attempted to stabilize the structure at atmospheric pressure, such as changing the damping parameters, or running a simulation with a gradual decrease in target pressure down to 1 atm, however the crystal structure continued to break down. To overcome this, the $\alpha\text{-S}_8$ system was also equilibrated using the ReaxFF force field parameterized by Järvi et al.^[24] This force field maintained the $\alpha\text{-S}_8$ crystallinity throughout equilibration (Figure 5b) and thus would be more appropriate for modelling a cathode structure with crystalline sulfur. However, it was only parameterized for C, S, H and Au elements, and thus could not be used to test cathode lithiation or cathode structure interfaces with an electrolyte. Instead, this force field was only used to equilibrate cathode structures and compare them with

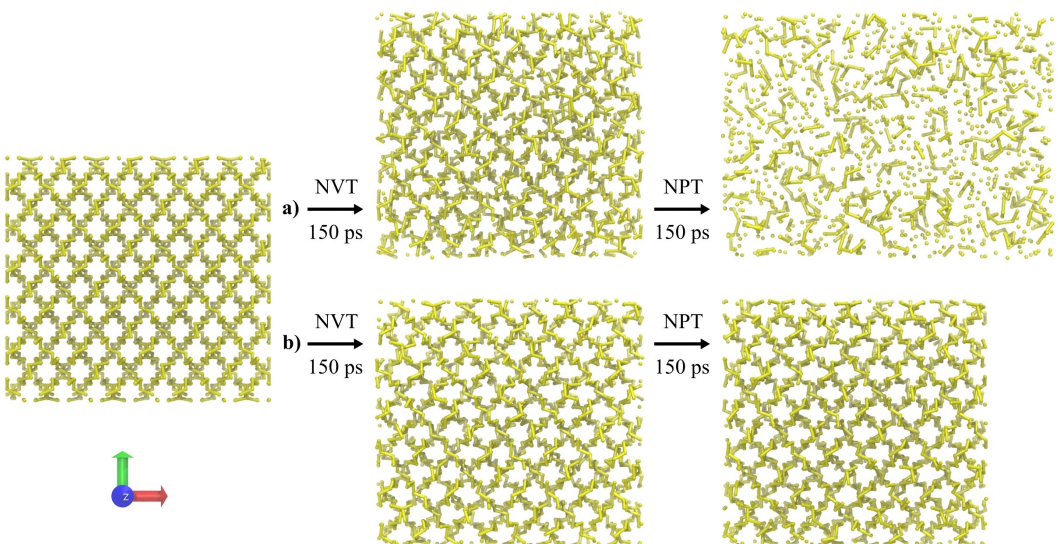


Figure 5. The crystal structure of α -S₈ alongside structures post-equilibration under NVT followed by NPT conditions with the ReaxFF force fields parameterized by a) Islam et al.,^[22] FF1-LiS, and b) Järvi et al.,^[24] FF2- α S.

the CAT01 and CAT02 structures produced by the Islam et al.^[22] force field. From here on, the force field parameterized by Islam et al.^[22] will be referred to as FF1-LiS, and that parameterized by Järvi et al.^[24] will be referred to as FF2- α S.

The differences in sulfur behavior between these two force fields can likely be explained by their intended use. FF2- α S was parameterized with the intention of reproducing both small sulfur-containing molecules and bulk system properties at a reasonable accuracy.^[24] The authors commented that this was quite difficult, given the high number of bulk allotropes and complex energy landscape of sulfur under different conditions. The potential they developed was successful in approximately reproducing the ground state orthorhombic α -S₈ crystal lattice at room temperature (300 K) with lattice parameters within 0.4 Å of the reference experimental unit cell (simulated cell dimensions: 10.1×12.8×24.2 Å). They reported a density of 2.16 g cm⁻³, which was consistent with the 2.134 g cm⁻³ density achieved in this study using the same force field on a super cell. These values also compare well with the experimental density of orthorhombic α -S₈ of 2.067 g cm⁻³.^[25]

FF1-LiS was parameterized starting from the C, H, O and S interactions of the 2012 Castro-Marcano ReaxFF force field used for modelling combustion and pyrolysis of an Illinois No. 6 coal char.^[26] These parameters were mainly based on small molecule sulfur species and sulfur-containing hydrocarbons. Given the complex energy landscape of sulfur, it appears FF1-LiS is appropriate for modelling sulfur-containing hydrocarbons but does not fully account for bulk crystalline behavior, resulting in the collapse of the α -S₈ crystal structure during NPT simulation.

Cathode structural characterization

The differences in crystalline sulfur behavior and reactivity between FF1-LiS and FF2- α S implies that equilibration of

graphene flakes and sulfur with these force fields would produce different cathode structures. To investigate these structural differences, the initial CAT01 and CAT02 structures (prior to equilibration using FF1-LiS) were also equilibrated using FF2- α S. In addition, a system with crystalline regions of α -S₈ in the initial configuration, dubbed CAT03, was equilibrated using both FF1-LiS and FF2- α S. The CAT03 system contained the same number of graphene flakes and S₈ rings as CAT02 (22 C₂₂ flakes, 22 C₄₂ flakes, and 116 S₈ rings), however the S₈ rings were in crystalline α -S₈ blocks (2 blocks of 24 S₈ molecules, and 4 blocks of 12 S₈ molecules, plus the remaining 20 individual S₈ rings). A diagram summarizing all the systems that were equilibrated and studied using the two different ReaxFF force fields is presented in Section S1 of the Supporting Information.

It was hypothesized that FF2- α S could potentially maintain the crystallinity in CAT03 throughout equilibration and appropriately model a cathode structure with crystalline sulfur (like those observed experimentally in references^[14a,b]). The initial structure and final equilibrated structures using FF1-LiS and FF2- α S for the CAT01, CAT02 and CAT03 systems are presented in Figure 6.

The chemical species present in the final cathode structures varied between FF1-LiS and FF2- α S equilibrations, particularly in respect to the sulfur species. Throughout the NVT and NPT thermal equilibration, the percentage of sulfur atoms present as short chain sulfur (S₁–S₈), S₈ rings, long chain sulfur (S_n where n > 8), and sulfur in a molecule bonded to carbon (S–C composite) were tracked using the TRAVIS software.^[34] The results for CAT01, CAT02 and CAT03 equilibration runs are presented in Figure 7. Across all cathode systems, the FF1-LiS equilibration showed a rapid conversion of sulfur initially in S₈ rings to produce various products including S–C composites, shorter chain degradation products (S₁–S₈), and long chain sulfur (S_n). Almost all the S₈ rings had completely reacted by 100 ps

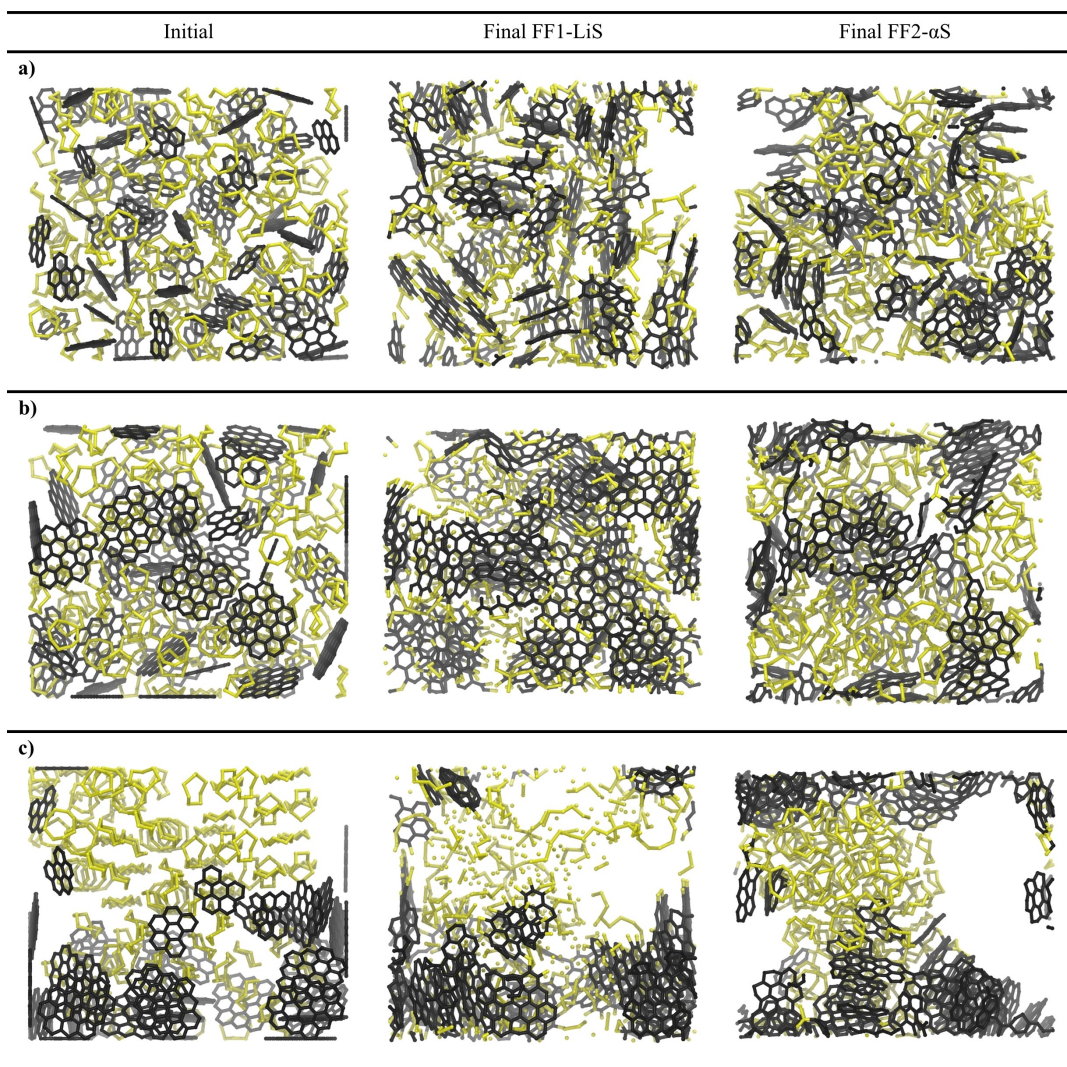


Figure 6. Initial and final equilibrated structures using FF1-LiS and FF2- α S for cathode systems a) CAT01, b) CAT02, and c) CAT03. Atoms represented by different colored spheres, C: black, and S: yellow.

into the MD simulation, and none remained after the full equilibration, further indicating that S_8 ring species are not stable when described by FF1-LiS. Equilibration of these systems using FF2- α S also showed reactions taking place and a decrease in sulfur atoms as S_8 rings; however, this decrease was much slower, and plateaued out by approximately 700 ps into the MD simulation. The percentage of sulfur atoms in S_8 rings remaining after equilibration was between 31% and 46%, which indicated S_8 ring species modelled using FF2- α S could maintain their stability even in the presence of graphene flakes. Despite their differences, both force fields produced voids when used to equilibrate the CAT03 structure, which is representative of models of a more porous material. Similar disparities in sulfur behavior between FF1-LiS and FF2- α S were also observed in the formation of short chain sulfur products (S_1-S_8) and S-C composites. All cathode systems equilibrated using FF1-LiS contained some short chain sulfur species in the final structure, ranging from 8 to 57% (CAT01 and CAT03 respectively). For the final CAT03 structure, 32% of sulfur atoms

existed as single atom sulfur (S_1) where the bonds from S_8 rings had dissociated. In contrast, equilibration with FF2- α S resulted in almost no short chain sulfur formation, and no short chain sulfur was present in any of the final structures. For the CAT01 and CAT02 systems, the percentage of sulfur atoms in S-C composites was higher using FF1-LiS (with the more reactive sulfur) compared to FF2- α S. This was not the case for CAT03, although the very large difference in the percentage of S_1-S_8 chains still indicated the increased reactivity of sulfur in FF1-LiS for this cathode system.

The RDF of C-C, C-S and S-S interactions was also calculated for each cathode system equilibrated with both force fields. The major differences in RDF results were observed when comparing the same cathode system equilibrated with different force fields. The results for the CAT02 system were representative of these force field effects and are presented in Figure 8 (see Section S2 of the supporting information for CAT01 and CAT03 RDF results). The first shell C-C peak was observed at 1.425 and 1.475 Å for the FF1-LiS and FF2- α S equilibrated

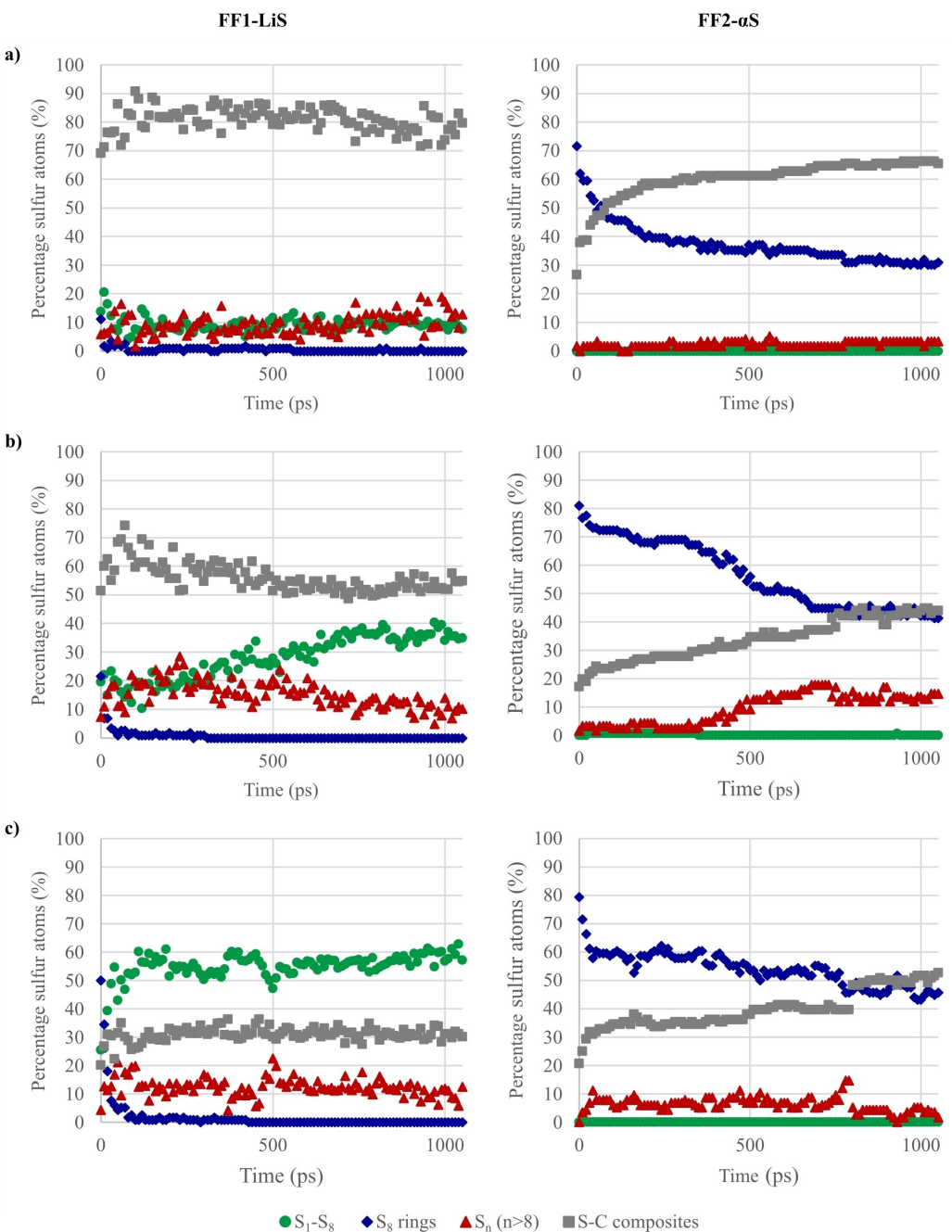


Figure 7. The percentage of sulfur atoms within molecules of short chain sulfur (S_1 – S_8), S_8 rings, long chain sulfur (S_n where $n > 8$), and sulfur in a molecule bonded to carbon (S–C composites) throughout the NVT and NPT stages of cathode thermal equilibration. Results include equilibration using FF1-LiS and FF2- α S for a) CAT01, b) CAT02, and c) CAT03 systems.

structures, respectively. These are in agreement with the literature value of 1.40 Å reported as the typical C–C bond length observed in a graphene sheet.^[15] Additional C–C peaks centered around 2.525 and 2.925 Å correspond to the second and third shell distances between carbon atoms on the same graphene flake. The other noticeable C–C maximum of $g(r)$ at 3.825 Å represents the typical atomic distance between stacked graphene flakes, which were observed during these simulations. This interatomic distance agrees with the expanded graphite (EG) interlayer spacing of 3.8 Å reported by Wang et al.^[13b] for a

series of LSB cathodes prepared using the melt diffusion method.

The RDF of C–S and S–S interactions varied between the two force fields. The only major C–S peak was centered around 1.775 Å for both structures, but the peak was much lower in intensity in the structure equilibrated using FF2- α S. This supports the presence of fewer C–S bonds in this structure due to the decreased reactivity of sulfur using these parameters. For the CAT02 structure equilibrated with FF1-LiS, the first shell peak in the S–S RDF was observed at 2.175 Å, and broadly

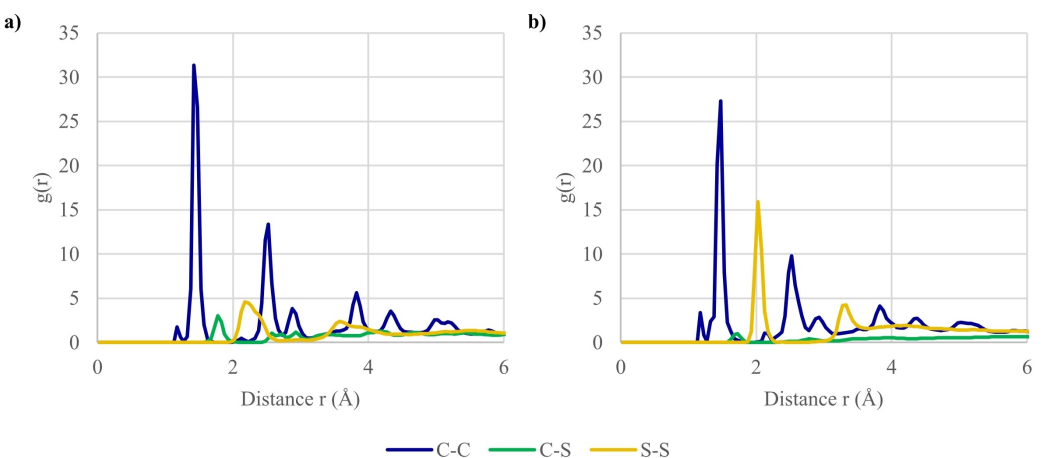


Figure 8. RDF, $g(r)$, of the C–C (blue line), C–S (green line), and S–S (yellow line) interactions of the CAT02 system equilibrated using a) FF1-LiS and b) FF2- α S.

tailed off toward larger interatomic distances (Figure 8a). The CAT02 structure equilibrated with FF2- α S exhibited an S–S RDF maximum at a shorter 2.025 Å, with a much sharper and more intense peak (Figure 8b). This suggests that the S–S bonds simulated using FF2- α S were stronger and experienced less bond stretching than those simulated using FF1-LiS. The shorter S–S bond length observed using FF2- α S is also more consistent with the literature reported value for S_8 rings (2.072 Å) obtained using density functional theory calculations.^[27] Longer and more varied S–S bond lengths such as those found in the FF1-LiS structure were more consistent with literature values for polysulfide chains of various lengths.^[27] This further supports the results obtained from the TRAVIS molecule analysis, which indicated that S_8 rings were stable and present in the final FF2- α S structures but broke apart into various polysulfide chains with longer bonds when using FF1-LiS.

The initial configuration of the CAT03 system contained blocks of crystalline α - S_8 , and thus after equilibration with FF2- α S, was expected to be the most likely cathode structure to contain crystalline sulfur regions. TRAVIS results showed this

structure after equilibration contained the highest proportion of sulfur atoms remaining in S_8 rings (46%). While the S_8 molecules were seen to cluster together (Figure 6c), it was unclear from visual assessment whether a crystalline α - S_8 configuration was present. The XRD pattern for this structure was calculated and compared to that of orthorhombic α - S_8 and a simulation box containing pure C_{22} and C_{42} graphene flakes (GF) equilibrated using FF2- α S (Figure 9a). A broad peak around 26° of 2θ in the pure graphene flake system was consistent with the experimental (002) reflection plane from an EG interlayer spacing of 3.8 Å.^[13b] Peaks in the range of 25°–30° of 2θ are also present in the α - S_8 system XRD pattern, but the more intense peak at 23° of 2θ from the (222) reflection plane (interatomic distance 3.85 Å^[25]) was considered as the characteristic indicator of crystalline sulfur. Comparison of these calculated spectra revealed that no α - S_8 remained in the CAT03 structure with an intense enough signal to indicate crystallinity in the XRD.

The CAT03 system equilibrated with FF2- α S was therefore not successful in modelling an experimental cathode with

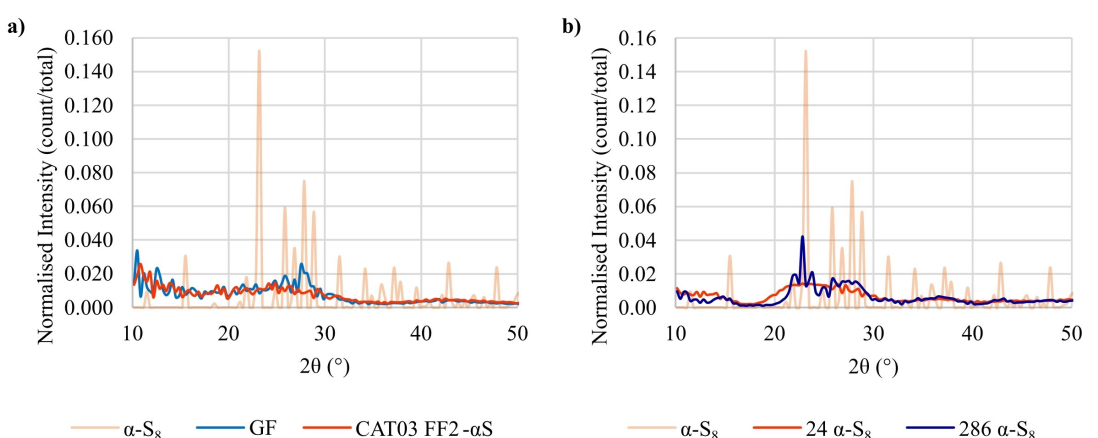


Figure 9. Calculated XRD patterns of a) the CAT03 final structure after equilibration with FF2- α S (red line), compared with crystalline orthorhombic α - S_8 (orange line) and a pure graphene flake (GF) system (blue line), and b) isolated blocks of 24 S_8 molecules (red line) and 286 S_8 molecules (blue line) in an α - S_8 configuration compared with a fully periodic α - S_8 crystalline system (orange line).

crystalline sulfur. However, further XRD calculations were performed on several different sized α -S₈ blocks, which revealed that to observe the sharp peak at 23° of 20, a crystal with at least 286 molecules of S₈ (equating to a crystal size of approximately 35 Å) was required (Figure 9b). This can be further verified using the Scherrer equation, which relates the XRD peak breadth at half-maximum (B_{hkl}) to the crystal size perpendicular to the hkl lattice plane (D_{hkl}) as

$$D_{hkl} = \frac{K\lambda}{B_{hkl}\cos\theta}, \quad (2)$$

where λ is the X-ray wavelength, θ is the Bragg angle, and K is a constant referred to as a crystallite-shape factor.^[28] The value of K can vary depending on crystal shape, but a value of 0.9 has been proposed as a reasonable approximation.^[28] Using the peak at 23° of 20 in the 286 α -S₈ block XRD pattern, a crystal size of 31 Å was calculated. This was consistent with the crystal block length of approximately 35 Å determined from visualization of the simulated system. The XRD pattern of the 24 α -S₈ block was much too broad to accurately determine crystallite size using the Scherrer equation, as the breadth of the peak overlapped with other reflections. By visualization of the system, the crystal size was approximated as 16 Å, which evidently was not large enough to produce an intense and distinguishable peak in the XRD.

This suggests that if a region of α -S₈ larger than 31 Å was simulated in a cathode system, some of this region may be able to withstand the reactive edges of the graphene flakes and maintain enough crystallinity in the cathode to be observed in the XRD pattern. However, such a simulation would involve a much larger system size and more computational time to equilibrate, which is likely pushing the limits of these ReaxFF simulations. Notably, in experimental XRD studies characterizing LSB cathode materials, the absence of sulfur peaks is usually interpreted as the absence of crystalline sulfur.^[13b] However, these results imply that a material could contain small nanocrystalline regions of α -S₈ even in the absence of the characteristic sulfur peaks in the XRD pattern.

Conclusions

This work revealed new information on the atomic level structure of LSB cathodes and their interface with a conventional organic electrolyte using reactive MD simulations. Investigating the effect of graphene flake size on cathode structure, it was found that the CAT01 system with smaller graphene flakes (C₁₆ and C₂₂ flakes) formed a highly amorphous structure with well dispersed sulfur and a high content of C–S bonds. The CAT02 system (with larger C₂₂ and C₄₂ flakes) formed a structure with more long chain sulfur species which were less bonded to the graphene flake framework. The larger graphene flakes in the CAT02 interface appeared to shield long-chain lithium polysulfides from migrating into the electrolyte, which would potentially help prevent the polysulfide shuttle effect. CAT01 may also contain structural features which mitigate this

shuttle, as literature has suggested that increased C–S bonding can anchor polysulfides to the carbon framework and prevent their dissolution into electrolyte.^[9] Further simulation is required to determine which structure is more effective in preventing the polysulfide shuttle effect.

Upon investigation of a crystalline α -S₈ system, it was found that the ReaxFF force field previously applied to LSB systems was unable to maintain crystalline α -S₈ during a simulation under constant pressure conditions. An alternative ReaxFF force field was found to achieve stable S₈ structures in a LSB cathode environment, but it lacked the parameters for lithium and other elements required to effectively model interfaces with electrolyte. These results highlight the need for improved methods of modelling LSB cathode structures to produce more accurate and useful information at the atomic level.

Finally, it was found that nanocrystalline regions of α -S₈ with crystal sizes up to 31 Å may be present despite a lack of characteristic peaks in XRD analysis. This further emphasizes the need for more accurate simulations to determine whether, and to what extent, such regions occur under experimental conditions.

Methods

MD using ReaxFF

The ReaxFF reactive force field calculates the total energy of the system from a series of contributing terms.

$$E_{\text{system}} = E_{\text{bond}} + E_{\text{over}} + E_{\text{angle}} + E_{\text{tors}} + E_{\text{vdw}} + E_{\text{Coulomb}} + E_{\text{specific}}, \quad (3)$$

where E_{bond} is the bond energy, E_{over} is an energy penalty for over-coordinated atoms, E_{angle} is the angle strain energy, E_{tors} is the torsion angle energy, E_{vdw} is the van der Waals energy, and E_{Coulomb} is the Coulombic energy.^[29] Several different versions of the ReaxFF force field have been parameterized since its development, with added energy terms that are specific to the system being simulated (such as lone pair or conjugation contributions).^[22,24] These extra terms are all grouped under E_{specific} in Equation (3). The other variables in Equation (3) can be divided into bond order (BO) dependent and BO independent terms, all calculated from atomic positions. Unlike non-reactive force fields, these BO dependent terms allow for ReaxFF to model reactive events.

The BO between two atoms, i and j, is given by the equation:

$$\text{BO}_{ij} = \exp\left[\rho_{bo1}\left(\frac{r_{ij}}{r_o^\sigma}\right)^{\rho_{bo2}}\right] + \exp\left[\rho_{bo3}\left(\frac{r_{ij}}{r_o^\pi}\right)^{\rho_{bo4}}\right] + \exp\left[\rho_{bo5}\left(\frac{r_{ij}}{r_o^{\pi\pi}}\right)^{\rho_{bo6}}\right], \quad (4)$$

where r_{ij} is the interatomic distance between atoms i and j, the r_o terms are the equilibrium bond lengths for σ , π and $\pi\pi$ type bonds, and the ρ_{bo} terms are empirical parameters (note ρ_{bo1} , ρ_{bo3} and ρ_{bo5} are negative).^[29] The BO dependent energy terms (E_{bond} , E_{over} , E_{angle} , E_{tors}) disappear smoothly upon bond dissociation, treating chemical bonding implicitly based on interatomic distances and allowing reactions to take place during simulations. ReaxFF also treats all atoms, bonded and non-bonded, with Coulombic (E_{Coulomb}) and

distance-corrected Morse (E_{vdw}) potentials, which are independent of bond order.^[22] $E_{Coulomb}$ is calculated from partial atomic charges derived using the electronegativity equalization method (EEM).^[29]

The ReaxFF force field is parameterized against large QM datasets and/or experimental values to model atomic interactions effectively.^[30] The present work employed the ReaxFF force field parameterized by Islam et al.,^[22] and then a later one parameterized by Järvi et al.^[24] for comparison. The force field parameters are given in the Section S3 of the supporting information.

Simulation details

All MD simulations were run in LAMMPS^[23] and used a periodic simulation box and a timestep of 0.25 fs. Following methods adapted from the literature,^[3,16] the cathode systems were first minimized at 0 K using the Polak-Ribiere conjugate gradient algorithm^[31] until the change in energy between iterations was less than 0.0001%. These structures were then heated to 300 K using a Langevin thermostat^[32] at a rate of 25 Kps⁻¹ and under constant volume conditions. The systems then underwent a two-stage thermal equilibration. First, a 150 ps simulation under NVT (constant number of particles, volume, and temperature) conditions at 300 K was performed using a Nosé-Hoover chain thermostat with a chain length of 3, and with a temperature damping parameter of 25 fs. Secondly, the structures were equilibrated under anisotropic NPT (constant number of particles, pressure, and temperature) conditions for 900 ps, using a Nosé-Hoover chain thermostat and barostat (chain length of 3) at 300 K and 1 atm, respectively, with a pressure damping parameter of 250 fs. For an orthogonal simulation box in LAMMPS, anisotropic NPT conditions allow the lattice vectors to vary independently, while keeping the angles constant.

Cathode-electrolyte interfaces were also simulated for the CAT01 and CAT02 systems. Two electrolyte simulation boxes with approximately 1.2 M lithium in DOL solvent (a common organic solvent used in electrolytes of LSBs^[6b,14b]) were built to the final x and y dimensions of the cathodes post-equilibration, and 30 Å wide in the z dimension. These boxes contained 380 DOL solvent molecules and 33 Li atoms. The electrolyte was minimized and then heated to 300 K using the ReaxFF force field parameterized by Islam et al.^[22] and the method described above. The equilibrated electrolyte and the electrode simulation cells were joined on the z axis, with a 3 Å gap between them, and atom coordinates were adjusted such that any molecules which previously crossed a periodic boundary remained intact. The combined system was then simulated under anisotropic NPT conditions at 300 K and 1 atm for 300 ps. Cathode structures and cathode-electrolyte interfaces were considered equilibrated when the total energy of the system had plateaued, where the average change in energy across the last 200 ps of simulation was less than 0.002 kJ mol⁻¹ (see Section S4 of the supporting information).

To test the ability of ReaxFF to simulate crystalline systems, an equilibration simulation was also performed on a supercell structure of crystalline orthorhombic α -S₈ built from experimental X-ray data^[25] (supercell dimensions: 42×39×24 Å). The experimental structure used for initial coordinates was measured at 298 K and did not require minimization or heating steps. This system was equilibrated under NVT conditions at 300 K for 150 ps using a Nosé-Hoover chain thermostat (with a chain length of 3), followed by anisotropic NPT conditions at 300 K and 1 atm for 150 ps using a Nosé-Hoover chain thermostat and barostat (with chain lengths of 3).

MD simulation trajectories were visualized using the Visual Molecular Dynamics (VMD, version 1.9.4) software.^[33] Molecule detection across the simulation time was performed using TRAVIS –

Trajectory Analyzer and Visualizer.^[34] XRD patterns for all systems were computed in LAMMPS, specifying a copper wavelength (λ) of 1.541838 Å.^[35]

Acknowledgements

The authors thank the Australian Research Council for its support for this project through the Discovery program (FL190100080). T.D. acknowledges support from the Australian Government through an Australian Government Research Training Program Scholarship and the University of Queensland's School of Chemistry and Molecular Biosciences (SCMB) and Australian Institute for Bioengineering and Nanotechnology (AIBN) for financing a SCMB Honours Scholarship. We acknowledge access to computational resources provided by the Pawsey Supercomputing Centre with funding from the Australian Government and the government of Western Australia; and the National Computational Infrastructure (NCI Australia), an NCRIS enabled capability supported by the Australian Government. We also acknowledge support from the Queensland Cyber Infrastructure Foundation (QCIF), high performance computing support from Dr Emily Kahl and useful discussion with Prof Ian R. Gentle. Open Access publishing facilitated by The University of Queensland, as part of the Wiley - The University of Queensland agreement via the Council of Australian University Librarians.

Conflict of Interests

There are no conflicts to declare.

Data Availability Statement

The data that support the findings of this study are available from the corresponding author upon reasonable request.

Keywords: cathode materials · electrochemistry · graphene flake · lithium-sulfur (Li–S) batteries · molecular dynamics

- [1] a) S.-H. Chung, A. Manthiram, *Adv. Mater.* **2019**, *31*, 1901125; b) A. Manthiram, Y. Fu, S.-H. Chung, C. Zu, Y.-S. Su, *Chem. Rev.* **2014**, *114*, 11751–11787.
- [2] E. M. Erickson, C. Ghanty, D. Aurbach, *J. Phys. Chem. Lett.* **2014**, *5*, 3313–3324.
- [3] S. Perez Beltran, P. B. Balbuena, *ChemSusChem* **2018**, *11*, 1970–1980.
- [4] W. Deng, J. Phung, G. Li, X. Wang, *Nano Energy* **2021**, *82*, 105761.
- [5] a) H.-J. Peng, J.-Q. Huang, X.-B. Cheng, Q. Zhang, *Adv. Energy Mater.* **2017**, *7*, 1700260; b) F. Zhao, J. Xue, W. Shao, H. Yu, W. Huang, J. Xiao, *J. Energy Chem.* **2023**, *80*, 625–657.
- [6] a) S. Lang, S.-H. Yu, X. Feng, M. R. Krumov, H. D. Abruna, *Nat. Commun.* **2022**, *13*, 4811; b) J. C. Burgos, P. B. Balbuena, J. A. Montoya, *J. Phys. Chem. C* **2017**, *121*, 18369–18377.
- [7] Z.-L. Xu, J.-K. Kim, K. Kang, *Nano Today* **2018**, *19*, 84–107.
- [8] X. Xu, S. Wang, H. Wang, B. Xu, C. Hu, Y. Jin, J. Liu, H. Yan, *J. Energy Storage* **2017**, *13*, 387–400.
- [9] S. Evers, L. F. Nazar, *Acc. Chem. Res.* **2013**, *46*, 1135–1143.

- [10] X. Li, Y. Cao, W. Qi, L. V. Saraf, J. Xiao, Z. Nie, J. Mietek, J.-G. Zhang, B. Schwenzer, J. Liu, *J. Mater. Chem.* **2011**, *21*, 16603–16610.
- [11] a) L.-P. Hou, X.-Q. Zhang, N. Yao, X. Chen, B.-Q. Li, P. Shi, C.-B. Jin, J.-Q. Huang, Q. Zhang, *Chem* **2022**, *8*, 1083–1098; b) C. Li, R. Liu, Y. Xiao, F. Cao, H. Zhang, *Energy Storage Mater.* **2021**, *40*, 439–460; c) C. Fu, M. B. Oviedo, Y. Zhu, A. von Wald Cresce, K. Xu, G. Li, M. E. Itkis, R. C. Haddon, M. Chi, Y. Han, B. M. Wong, J. Guo, *ACS Nano* **2018**, *12*, 9775–9784; d) C. Fu, L. Xu, F. W. Aquino, A. v. Cresce, M. Gobet, S. G. Greenbaum, K. Xu, B. M. Wong, J. Guo, *J. Phys. Chem. Lett.* **2018**, *9*, 1739–1745.
- [12] E. P. Kamphaus, P. B. Balbuena, *J. Phys. Chem. C* **2016**, *120*, 4296–4305.
- [13] a) Y. Feng, H. Zhang, Y. Zhang, X. Qu, *ACS Omega* **2019**, *4*, 16352–16359; b) Y.-X. Wang, L. Huang, L.-C. Sun, S.-Y. Xie, G.-L. Xu, S.-R. Chen, Y.-F. Xu, J.-T. Li, S.-L. Chou, S.-X. Dou, S.-G. Sun, *J. Mater. Chem.* **2012**, *22*, 4744–4750; c) J.-Z. Wang, L. Lu, M. Choucair, J. A. Stride, X. Xu, H.-K. Liu, *J. Power Sources* **2011**, *196*, 7030–7034.
- [14] a) S. Zhang, W. Xiao, Y. Zhang, K. Liu, X. Zhang, J. Zhao, Z. Wang, P. Zhang, G. Shao, *J. Mater. Chem. A* **2018**, *6*, 22555–22565; b) A. D. Dysart, J. C. Burgos, A. Mistry, C.-F. Chen, Z. Liu, C. N. Hong, P. B. Balbuena, P. P. Mukherjee, V. G. Pol, *J. Electrochem. Soc.* **2016**, *163*, A730–A741; c) Z. Du, J. Xu, S. Jin, Y. Shi, C. Guo, X. Kong, Y. Zhu, H. Ji, *J. Power Sources* **2017**, *341*, 139–146; d) P. Kumar, F.-Y. Wu, L.-H. Hu, S. Ali Abbas, J. Ming, C.-N. Lin, J. Fang, C.-W. Chu, L.-J. Li, *Nanoscale* **2015**, *7*, 8093–8100.
- [15] S. Perez Beltran, P. B. Balbuena, *J. Mater. Chem. A* **2018**, *6*, 18084–18094.
- [16] V. Ponce, J. M. Seminario, *J. Electrochem. Soc.* **2020**, *167*, 100555.
- [17] C. Arneson, Z. D. Wawrzyniakowski, J. T. Postlewaite, Y. Ma, *J. Phys. Chem. C* **2018**, *122*, 8769–8779.
- [18] M. D. Hanwell, D. E. Curtis, D. C. Lonie, T. Vandermeersch, E. Zurek, G. R. Hutchison, *J. Cheminformatics* **2012**, *4*, 1–17.
- [19] T. A. Halgren, *J. Comput. Chem.* **1996**, *17*, 520–552.
- [20] A. K. Rappe, C. J. Casewit, K. S. Colwell, W. A. Goddard, W. M. Skiff, *J. Am. Chem. Soc.* **1992**, *114*, 10024–10035.
- [21] L. Martínez, R. Andrade, E. G. Birgin, J. M. Martínez, *J. Comput. Chem.* **2009**, *30*, 2157–2164.
- [22] M. M. Islam, A. Ostadhossein, O. Borodin, A. T. Yeates, W. W. Tipton, R. G. Hennig, N. Kumar, A. C. T. van Duin, *Phys. Chem. Chem. Phys.* **2015**, *17*, 3383–3393.
- [23] A. P. Thompson, H. M. Aktulga, R. Berger, D. S. Bolintineanu, W. M. Brown, P. S. Crozier, P. J. in't Veld, A. Kohlmeyer, S. G. Moore, T. D. Nguyen, R. Shan, M. J. Stevens, J. Tranchida, C. Trott, S. J. Plimpton, *Comput. Phys. Commun.* **2022**, *271*, 108171.
- [24] T. T. Järvi, A. C. T. van Duin, K. Nordlund, W. A. Goddard, *J. Phys. Chem. A* **2011**, *115*, 10315–10322.
- [25] S. Rettig, J. Trotter, *Acta Crystallogr. Sect. C* **1987**, *43*, 2260–2262.
- [26] F. Castro-Marcano, A. M. Kamat, M. F. Russo, A. C. T. van Duin, J. P. Mathews, *Combust. Flame* **2012**, *159*, 1272–1285.
- [27] L. Wang, T. Zhang, S. Yang, F. Cheng, J. Liang, J. Chen, *J. Energy Chem.* **2013**, *22*, 72–77.
- [28] U. Holzwarth, N. Gibson, *Nat. Nanotechnol.* **2011**, *6*, 534–534.
- [29] A. C. T. van Duin, S. Dasgupta, F. Lorant, W. A. Goddard, *J. Phys. Chem. A* **2001**, *105*, 9396–9409.
- [30] M. M. Islam, V. S. Bryantsev, A. C. T. van Duin, *J. Electrochem. Soc.* **2014**, *161*, E3009–E3014.
- [31] J. R. Shewchuk, *An Introduction to the Conjugate Gradient Method without the Agonizing Pain*, Carnegie-Mellon University. Department of Computer Science Pittsburgh, 1994.
- [32] T. Schneider, E. Stoll, *Phys. Rev. B* **1978**, *17*, 1302–1322.
- [33] W. Humphrey, A. Dalke, K. Schulten, *J. Mol. Graphics* **1996**, *14*, 33–38.
- [34] a) M. Brehm, B. Kirchner, *J. Chem. Inf. Model.* **2011**, *51*, 2007–2023; b) M. Brehm, M. Thomas, S. Gehrke, B. Kirchner, *J. Chem. Phys.* **2020**, *152*, 164105.
- [35] a) S. Coleman, D. Spearot, L. Capolungo, *Modell. Simul. Mater. Sci. Eng.* **2013**, *21*, 055020; b) E. Prince, *International Tables for Crystallography, Volume C: Mathematical, Physical and Chemical Tables*, Springer Science & Business Media, 2004; c) L.-M. Peng, G. Ren, S. Dudarev, M. Whelan, *Acta Crystallogr. Sect. A* **1996**, *52*, 257–276.

Manuscript received: July 24, 2023

Revised manuscript received: October 5, 2023

Accepted manuscript online: October 13, 2023

Version of record online: November 9, 2023